

Computer-Aided Diagnosis of Low Grade Endometrial Stromal Sarcoma (LGESS)

Xinxin Yang* Mark Stamp*†

July 13, 2021

Abstract

Low grade endometrial stromal sarcoma (LGESS) is rare form of cancer, accounting for about 0.2% of all uterine cancer cases. Approximately 75% of LGESS patients are initially misdiagnosed with leiomyoma, which is a type of benign tumor, also known as fibroids. In this research, uterine tissue biopsy images of potential LGESS patients are preprocessed using segmentation and staining normalization algorithms. A variety of classic machine learning and leading deep learning models are then applied to classify tissue images as either benign or cancerous. For the classic techniques considered, the highest classification accuracy we attain is about 0.85, while our best deep learning model achieves an accuracy of approximately 0.87. These results indicate that properly trained learning algorithms can play a useful role in the diagnosis of LGESS.

1 Introduction

Cancer is the second leading cause of death in the United States, accounting for 21.6% of all deaths in a 2017 survey conducted by the Center for Disease Control (CDC) [19]. The tremendous medical costs of cancer treatments and the harm the disease brings to patients and their families makes cancer an important area of medical research.

Low grade endometrial stromal sarcoma (LGESS) is a tumor comprised of endometrial stromal cells. It is rare, accounting for approximately 0.2% of uterine cancers [7, 20]. Most patients with LGESS have a good prognosis, with a 5-year survival rate of about 80% after surgical removal of the tumor. However, LGESS has a relatively high recurrence rates. at about 60%, and the disease-related death rate is estimated to be between 15% and 25% [15, 32].

*Department of Computer Science, San Jose State University

†mark.stamp@sjsu.edu

When diagnosing LGESS, it is difficult to differentiate LGESS from benign leiomyoma, which is also known as fibroids. Only 10% of LGESS patients are correctly diagnosed, whereas 75% are misdiagnosed with preoperative leiomyoma [22]. Many cases even remain misdiagnosed postoperative [11]. More accurate and automatic image analysis methods would be useful to diagnose LGESS, assess treatment efficacy, and lower cancer-related costs to the healthcare system.

Researchers in artificial intelligence (AI) rarely possess the medical knowledge required for accurate modeling a disease such as LGESS. And AI algorithms that are less than 100% accurate make such techniques more suited as an aid in cancer risk assessment, rather than definitive diagnostic tools [25]. Learning models can reduce the workload of healthcare professionals by automating tedious tasks, such as tumor segmentation. Moreover, AI algorithms may be more capable than humans at analyzing smaller, more subtle structures in patient images [1]. Also, computers can analyze larger feature sets in a shorter amount of time, potentially allowing for a more nuanced analysis of image structure that is not easily perceived by a human viewer. These capabilities have been showcased in a wide variety of use cases, including tumor segmentation, determination of tumor malignancy, and prediction of survivability in afflicted patients [27].

In this research, we apply machine learning and deep learning methods to classify soft tissue images of potential LGESS patients. Our goal is to provide tools for improved diagnostic accuracy of LGESS tumors.

The remainder of this paper is organized as follows: Section 2 contains relevant background material, including a review of research literature related to cancer image analysis, and a brief introduction to the machine learning and deep learning algorithms that we employ in our LGESS experiments. Specifically, we consider classic machine learning techniques of multilayer perceptron (MLP), random forest, XGBoost, support vector machines (SVM), principal component analysis (PCA) in combination with SVM. In the realm of deep learning algorithms, we consider convolutional neural networks (CNN), residual networks (ResNet), AlexNet, and DenseNet.

Section 3 gives an overview of the cancer image dataset used in this research, and we discuss the preprocessing strategies that we employ. This data preprocessing workflow includes region of interest (ROI) segmentation, image patch extraction, and stain normalization. In Section 4, we provide details on our machine learning and deep learning experiments, and we analyze the results. Section 5 concludes the paper, and we provide suggestions for possible future work to help diagnose LGESS based on image analysis.

2 Background

In this section, we discuss relevant background topics. First, we discuss relevant related work, then we provide a brief overview of each of the classic machine learning and deep learning algorithms that we employ for the analysis of LGESS images.

2.1 Related work

Machine learning has found widespread use in cancer classification and diagnosis [27, 17]. Although machine and deep learning research has been conducted on many different cancers, we are aware of no existing studies pertaining to LGESS. This may be due to the rarity of LGESS, as compared to other cancers that are typically studied in this type of research.

Mesrabadi and Faez [29] apply artificial neural networks (ANN), AlexNet, and support vector machines (SVM) to classify prostate cancer. In their experiments, AlexNet yielded a classification accuracy of 86.3%, compared to 81.1% for SVM and 79.3% from ANNs. Kharya et al. [23] note that generic ANNs are the most widely used prediction technique in medical forecasting, but the structure of such models is difficult to understand. Kharya et al. also consider the relative advantages and disadvantages of decision trees, naïve Bayes, ANNs and SVMs for breast cancer detection.

Ashhar et al. [4] consider the efficacy of deep learning algorithms for early detection of lung cancer. Lung cancer is almost always diagnosed at advanced stages—early and accurate screening would be beneficial to patient outcomes. Ashhar et al. apply five state-of-the-art CNN-based architectures to a dataset of computer tomography (CT) lung cancer images. They find that GoogleNet gives the best results, with an accuracy, specificity, sensitivity, and AUC of 94.53%, 99.06%, 65.67%, and 86.84%, respectively.

Vijayarajeswari et al. [36] apply Hough transforms to mammogram images to detect features that are potentially indicative of breast cancer. The images are then classified using SVM. They attain a 94% accuracy with this strategy, far surpassing the classification accuracy of SVM on unmodified images. The Wisconsin diagnostic breast cancer (WDBC) dataset was used as the source of their images [33].

In [16], Ghoneim et al. conduct research on cervical cancer detection and classification—cervical cancer is one of the leading causes of cancer death among women. They extract relevant features from cervical cancer images using CNNs, then classify the images using extreme learning machines (ELM), multi-layer perceptrons (MLP) and autoencoder (AE) based classifiers. The best performance in these experiments came from a CNN-ELM-based system, which attained an accuracy of 99.5% accuracy on a binary classification problem and 91.2% accuracy on a multiclass problem.

Chaturvedi et al. [12] propose a classification method for skin cancer that achieves better evaluation results than previous studies and exceeds human dermatologists. Their implementation of the MobileNet model achieved an overall accuracy of 83.1% for multiclass experiments involving seven classes.

Bharat et al. [6] apply traditional machine learning classifiers, including k -nearest neighbor (k -NN), naïve Bayes, classification and regression trees (CART), and SVMs to the problem of predicting and diagnosing breast cancer. They conclude that these machine learning algorithms behave quite differently depending on the application. Specifically, they find that k -NN has the best diagnostic results,

while naïve Bayes and logistic regression perform well when applied to specific breast cancer diagnosis problems. These results generally agree with the research of Rana et al. [31].

According to Maglogiannis et al. [26], SVM is the best technique for predicting recurrence or non-recurrence of breast cancer. In their research, SVM attains an accuracy of 96.91%, specificity of 97.67%, and sensitivity of 97.84%, outperforming the Bayesian and ANN classifiers it was compared against.

The results of these studies paint a promising picture for the predictive abilities of machine learning and deep learning in the cancer domain. In this research, we consider deep learning and machine learning for the diagnosis of LGESS based on image analysis.

2.2 Learning Algorithms

Based on our literature review, we will consider both classic machine learning models and various cutting-edge deep learning techniques. In this section, we provide a brief description of each learning model that we employ in our classification experiments.

2.2.1 Multilayer Perceptron

Multilayer perceptrons (MLP) are a type of artificial neural network (ANN). An MLP includes an input layer, an output layer, with one or more hidden layers in between. MLPs can form the basis for so-called deep neural networks (DNN), where multiple hidden layers are used [37].

2.2.2 Random Forest

A random forest combines multiple decision trees, where each component decision tree is trained on a subset of the data and features [8]. Every decision tree is itself a classifier, and hence if N decision trees comprise a random forest, we will have N classification results. A random forest typically uses a simple voting scheme among the component decision trees to determine the classification.

2.2.3 XGBoost

Extreme gradient boosting (XGBoost) [13] has attracted considerable attention because of its efficiency and high prediction accuracy. XGBoost is based on gradient boosted decision trees (GBDT) combined with various techniques designed to increase the efficiency, without compromising the accuracy.

2.2.4 SVM

Support vector machines (SVM) date to the early 1960s, but only became practical in the mid-1990s [5]. Prior to the recent re-emergence of deep learning, SVM was

regarded as one of the most successful machine learning algorithms, and it is still competitive in many problem domains.

In a binary classification problem, an SVM attempts to construct a separating hyperplane between the classes, while maximizing the “margin,” i.e., the minimum distance between the hyperplane and the training samples. The strength of SVMs derive largely from the so-called kernel trick, which enables us to work in a higher dimensional space—where there is a better chance of the data being linearly separable—without paying a significant performance penalty.

2.2.5 PCA

Principal component analysis (PCA) is one of the most widely used dimensionality reduction algorithms [34]. The PCA technique is based on eigenvalue analysis, with the underlying assumption being that linear combinations of features with larger variances are more relevant for classification than those with smaller variance.

2.2.6 CNN

As the name suggests, convolutional neural networks (CNN) include convolutional layers, which consist of filters that enable the efficient analysis of local structure [14]. Figure 1 illustrates a case where five convolutions are applied to three-dimensional data.

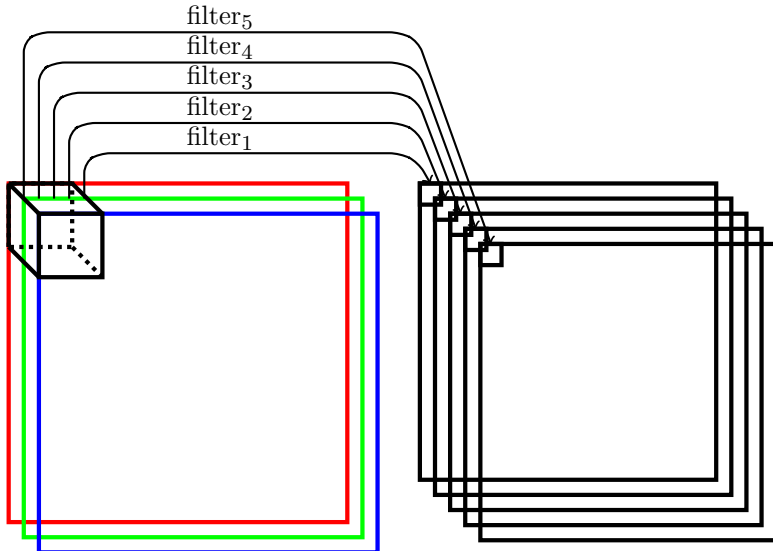


Figure 1: Convolution

By applying multiple convolutional layers, progressively higher levels of abstraction are obtained. CNNs were designed for image analysis, but the technique can perform well in any task where local structure dominates.

2.2.7 AlexNet

AlexNet is a specific CNN architecture. The AlexNet architecture is illustrated in Figure 2, as given in [24].

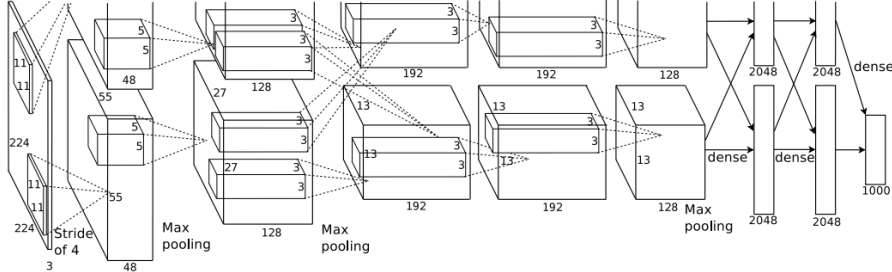


Figure 2: AlexNet architecture

From Figure 2, we see that AlexNet has eight layers, not including pooling layers, with the first five being convolutional layers, while the remainder are fully connected. There are 650,000 neurons and some 60 million parameters in AlexNet. See [24] for additional details on the AlexNet architecture.

2.2.8 DenseNet

The dense convolutional network (DenseNet) architecture was proposed in 2017 [21]. DenseNet connects each layer in a feed-forward manner. In contrast to a typical convolutional neural network, in DenseNet, the input of each layer includes the output of all previous layers. Figure 3 illustrates the DenseNet architecture, as given in [21].

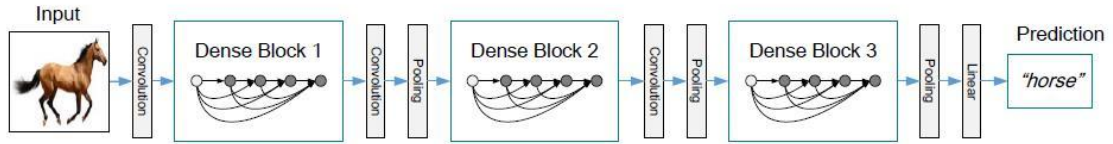


Figure 3: DenseNet architecture

2.2.9 ResNet

Residual networks (ResNet) were first proposed in 2015 when a ResNet architecture won first place in the classification task for the ImageNet competition. ResNet can be viewed as a collection of sub-networks that can be stacked to form a deep network. The use of these sub-networks, or “shortcut connections,” enables efficient training

of very deep networks [18]. Figure 4 illustrates a sub-network structure of ResNet. The identity mapping in Figure 4 represents a shortcut connection.

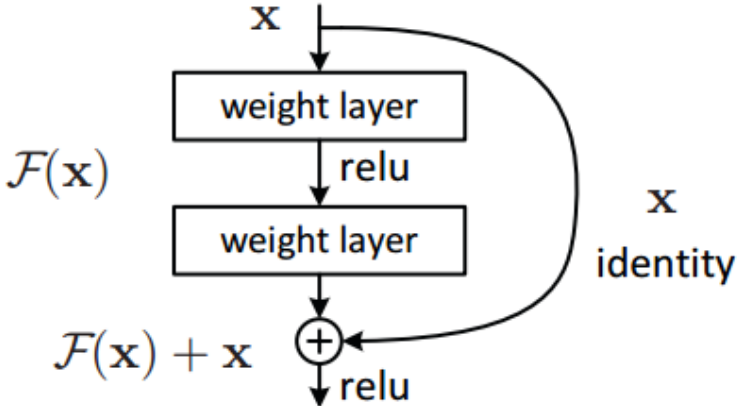


Figure 4: ResNet sub-network

3 Dataset and Preprocessing

The dataset used in our experiments was obtained from the Cancer Imaging Archive, an organization offering data for cancer research [10]. Our specific dataset includes 888 uterine tissue biopsy images taken from 250 potential LGESS patients, formatted as SVS files. A separate annotations file contains the clinical diagnosis of each tissue image.

SVS is a file format for whole slide images (WSI). In a WSI, a microscope slide is scanned to create a single high-resolution digital file [28]. Most WSIs have a resolution of $100,000 \times 100,000$ pixels. WSIs are usually stored in a pyramid structure, where each level of the pyramid holds different downsampled versions of the original image [9]. The more “downsampled” an image, the lower the resolution and the less magnified it appears to be. Figure 5 illustrates the pyramid structure of a WSI image. In this research, we use the OpenSlide library [30], which provides methods to read and access WSI images stored in a variety of file formats, including SVS.

WSIs offer clear visualization of tumor characteristics, including tissue infiltration, lymph node metastasis, and degree of differentiation. Such images are helpful for the diagnosis, prognosis, grading, and staging of tumors [35].

The WSIs contained in the Cancer Imaging Archive dataset must undergo a color standardization stage before our classification algorithms can be applied, since different production processes and scanning machines cause color variations. These color differences can cause problems for algorithms that are not robust to such variations, even if the differences are imperceptible to the human eye.

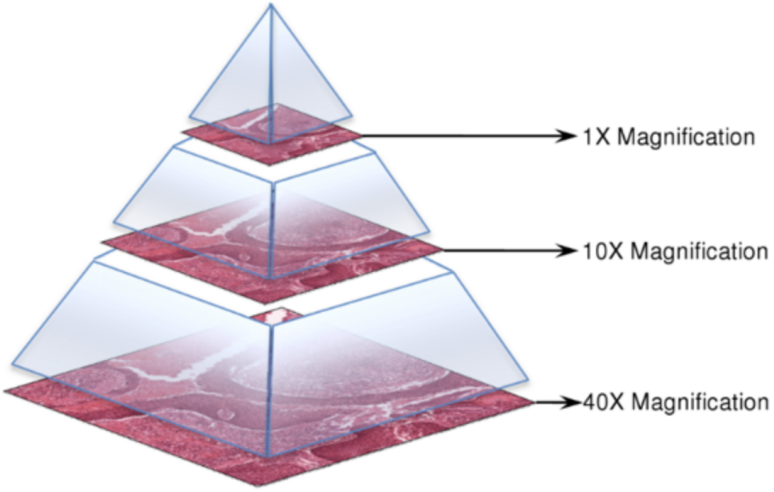


Figure 5: Whole slide image structure

The way we deal with these color difference is by color normalization, which is also referred to as stain normalization. This involves normalizing all pictures to the color distribution of the a template picture [3].

Before applying color normalization to our WSIs, the regions of interest (ROI) of each image need to be identified. This is done via standard Gaussian filtering and contour extraction techniques. The processing steps are explained in more detail below.

1. Segmentation of the target region from the image.

- (a) Use the OpenSlide library to read the level 2 image of the WSI. This second level of the WSI pyramid still has good resolution, but contains less data and is thus easier and more efficient to process. We save the level 2 image in portable network graphics (PNG) format.
- (b) Transform the image from the RGB color space to grayscale.
- (c) Apply a Gaussian filter to normalize the image. We must make sure the filter threshold preserves the image contours.
- (d) Calculate the area of each contour and remove all contours that have an area below a specified threshold.
- (e) Obtain the final image mask based on the contours acquired from the previous steps. This image mask comprises the tissue regions.

The Figure 6 below shows examples of extracted contours and the resulting image masks. In each row, the first image is the original image in the dataset, the second image is the mask we obtain from the original image, and the last image is the original image with the contours marked.

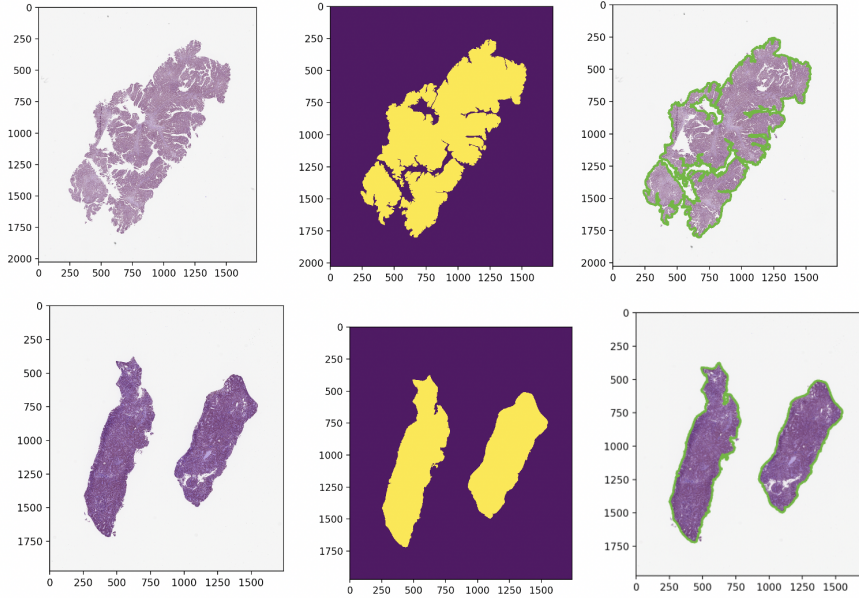


Figure 6: Contour and mask

2. Extract patches from an image's target region.

We apply the previously-generated mask to the image, then walk through the image and cut patches of a predefined length and width. All patches extracted must have a certain area occupied by the masked image. Patches below this area threshold consist mostly of empty space and are therefore discarded. Examples of extracted patches are given in Figure 7.

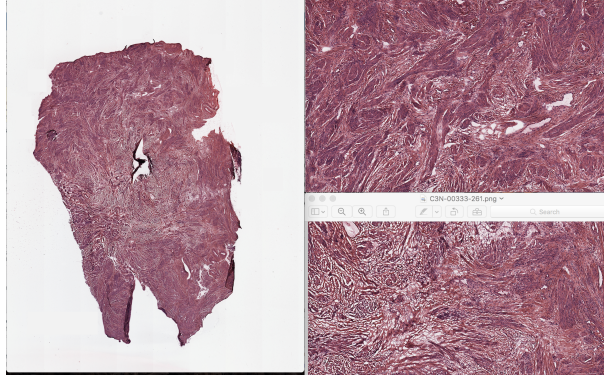


Figure 7: Patches cut from one image

3. Staining normalization.

We apply Vahadane's staining normalization to achieve color normalization [3]. The steps involved in this process are as follows:

- (a) Optical density calculation.
- (b) Unsupervised staining density estimation.
- (c) Color normalization.
- (d) Normalized pixel intensity calculation.

Examples of images before and after color normalization are given in Figure 8.

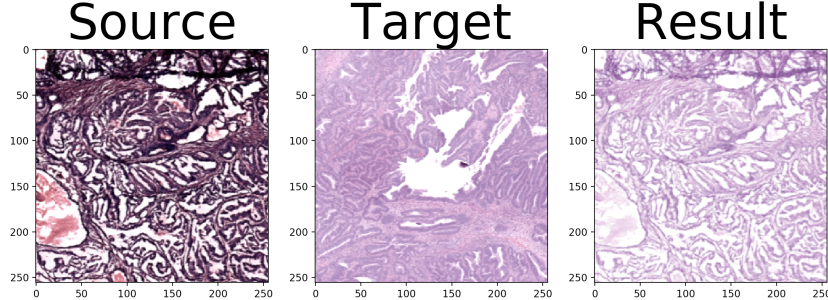


Figure 8: Color normalization of an image

Figure 8 shows the color of an original image, labeled “Source,” while the image labeled “Target” indicates the color we would like our image to become. The image labeled “Result” shows the original source image after color normalization. Note that the color of the “Result” image is similar to that of the “Target,” as desired.

Figure 9 shows 12 image examples from our dataset before and after color normalization. Note that in each case, the “before” image is directly above the corresponding “after” image.

Before normalization, we observe that the colors in the image can vary greatly. After our stain normalize process, the colors are clearly much more uniform.

4 Experiments and Results

After preprocessing the images and cutting them into patches, our dataset includes 4205 tumor images and 1459 benign images. We reserve 20% of the data as test data, while the remaining 80% data is used as training data, with the training and test data randomly selected. We also used 5fold cross validation to avoid overfitting problems. For each experiment, this gives us 4529 samples in the training set (3363 tumor images and 1166 benign images) and 1133 samples in the test set (841 tumor images and 292 benign images).

The metrics are used to evaluate the performance of our machine learning classifiers are precision, recall, F1 score, and the accuracy. Precision is the proportion of true positives among those predicted as positive, while recall measures how well the positive samples are predicted. In cancer detection, it is imperative that models

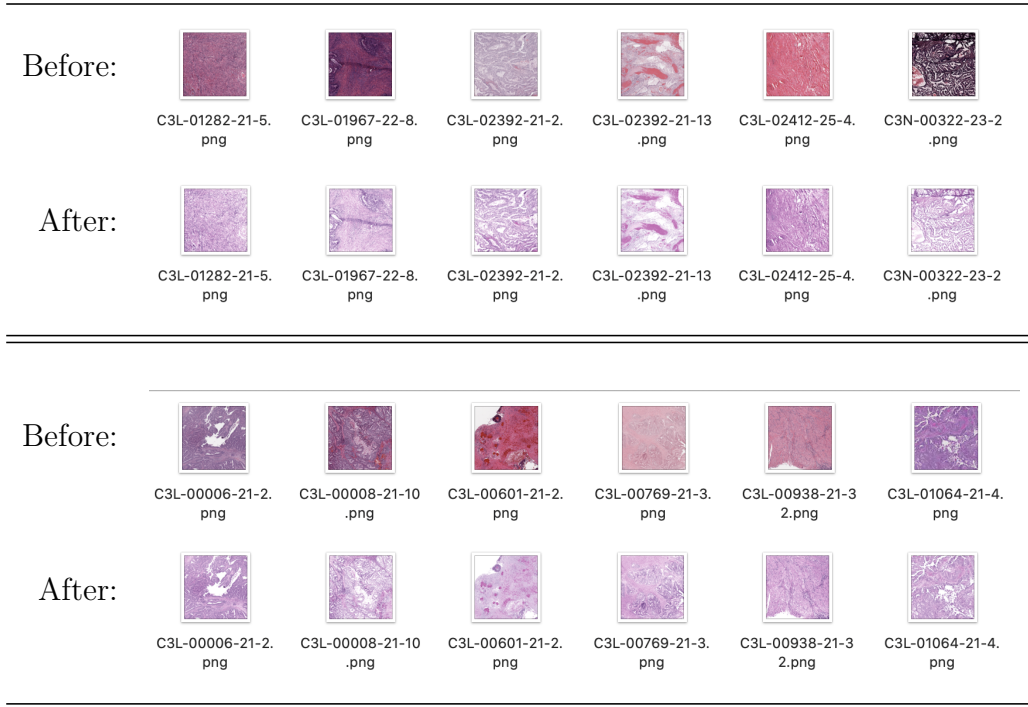


Figure 9: Color normalization examples

have a high recall. The F1 score is the harmonic of the precision and recall, while accuracy is self-explanatory.

For the basic techniques considered in the next section, we also provide ROC analysis. A receiver operating characteristic (ROC) curve is a plot of the true positive rate versus the false positive rate as the threshold varies through all possible values. The area under the ROC curve (AUC) can be interpreted as the probability that a randomly selected positive instance scores higher than a randomly selected negative instance. It follows that the AUC provides a threshold-independent means of comparing classifiers. An AUC of 1.0 implies that there is a threshold for which ideal separation is attained, while an AUC of 0.5 means that the binary classifier is no better than a coin flip. If an AUC value of $0 \leq x < 0.5$ is obtained, by simply switching the sense of the classifier, we have an AUC of $1 - x > 0.5$, and hence the AUC can be no worse than 0.5.

4.1 Basic Techniques

In this section, we will discuss our experiment result on “basic” or standard machine learning techniques. Here we include as basic MLP, random forest, XGBoost, and SVM models, as well as a model that combines PCA for dimensionality reduction with SVM. Here, we discuss the specific architecture for each of these models and

report the test accuracy. At the end of this section, we provide a more detailed comparison of these basic models.

4.1.1 Multilayer Perceptron

In this experiment, we imported `MLPClassifier` from the `Scikit-Learn` library. We use a fully connected neural network with three hidden layers—the first, second, and third hidden layers have 600, 800, and 300 neuron, respectively. We use rectified linear units (RELU) as the activation function for each neuron and we train the model for 600 epochs. In this case, we obtain a test accuracy of 0.5702.

4.1.2 Random Forest

We build our random forest model using `RandomForestClassifier` from the module `sklearn.ensemble`. We have experimented with the number of trees and find that 100 gives the best accuracy. Maximum depth of the tree was set to `None`, then the nodes were expanded until all leaves are pure or until all leaves contain less than 2. All other parameters of the model were set to default value. In this case, we obtain a test accuracy of 0.7873.

4.1.3 XGBoost

Our XGBoost model is trained using the `xgboost` package in Python. We obtain the best results with `max_depth` set to 6, and the objective function `binary:logistic`. We obtain a test accuracy of 0.8147.

4.1.4 Support Vector Machine

We use the SVM model from the `Scikit-Learn`. We found no significant difference between any kernel functions tested, and hence for the sake of efficiency, we select the linear kernel. We set all other parameters to default except enable the probability estimates. In our SVM experiment, we achieve a test accuracy of 0.8455.

4.1.5 PCA with SVM

In this experiment, we imported the PCA model from the `sklearn.decomposition` module. We combine the two models with the `make_pipeline` method from the `sklearn.pipeline` module. We find that we obtain the best results with 300 components from PCA and with the rbf kernel in the SVM. In this model, we again obtain a test accuracy of 0.8535.

4.1.6 Comparison of Basic Techniques

Table 1 we provide a more detailed comparison of the basic techniques considered above. The training and test accuracies are also given in the form of a bar graph

in Figure 10. We see that XGBoost, SVM, and PCA with SVM all yield an test accuracy of 0.85. The high training accuracy for random forest and XGBoost are indicative of overfitting.

Table 1: Accuracy, precision, recall, and F1 score for basic techniques

| Technique | Mode | Precision | Recall | F1 | Accuracy |
|---------------|-------|-----------|--------|--------|----------|
| MLP | Train | 0.7425 | 1.0000 | 0.8523 | 0.7425 |
| | Test | 0.7493 | 0.6326 | 0.6860 | 0.5702 |
| Random forest | Train | 0.7800 | 0.9795 | 0.8684 | 0.7796 |
| | Test | 0.7820 | 0.9893 | 0.8735 | 0.7873 |
| XGBoost | Train | 0.8254 | 0.9548 | 0.8854 | 0.8165 |
| | Test | 0.8171 | 0.9667 | 0.8856 | 0.8147 |
| SVM | Train | 0.8510 | 0.8598 | 0.8554 | 0.7847 |
| | Test | 0.8698 | 0.9301 | 0.8989 | 0.8455 |
| PCA with SVM | Train | 0.9201 | 0.9675 | 0.9432 | 0.8335 |
| | Test | 0.8567 | 0.9632 | 0.9068 | 0.8535 |

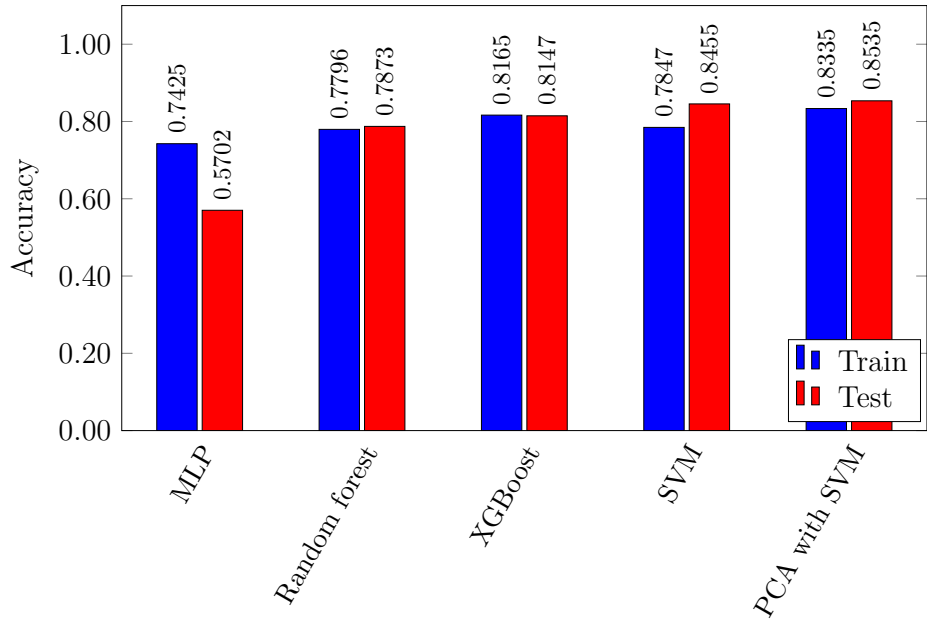


Figure 10: Accuracies for basic techniques

Figure 11 gives ROC curves for each of the basic classifiers considered above. By the AUC measure, SVM performs best, marginally outperforming the PCA with SVM model.

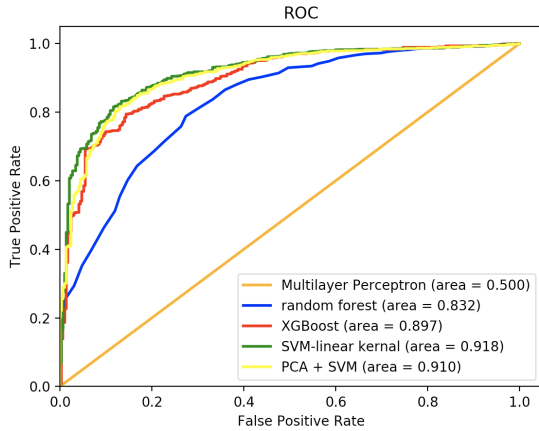


Figure 11: ROC analysis of basic classifiers

4.2 Advanced Techniques

In this section, we will discuss the performance of more advanced learning techniques. Specifically, we consider CNN, AlexNet, DenseNet, ResNet, and a ResNet model that includes realtime data augmentation.

4.2.1 Convolutional Neural Network

Our CNN model is implemented in `Tensorflow` and includes two convolution layers, a learning rate of 0.005, a `max_pool` size of two, and a final fully connected layer. We experimented with various batch sizes, number of generation, and optimizers. The loss and accuracy plots for our best result (which used the Adam optimizer) are shown in Figure 12. In this case, we have a training accuracy of 0.8143 test accuracy of 0.7860.

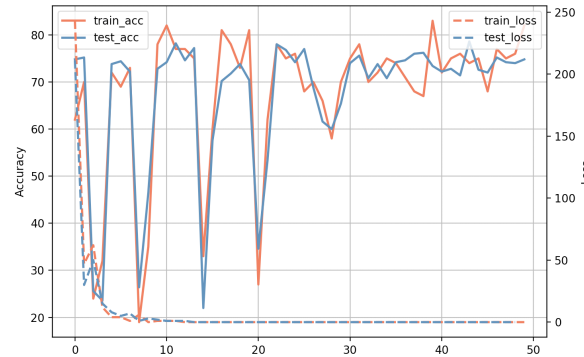


Figure 12: CNN performance

4.2.2 AlexNet

We use the original AlexNet architecture with a learning rate of 0.001, softmax as the loss function, and the Adam optimizer. We trained the model for 50 epochs. The best train and test accuracy we attain with AlexNet on our LGESS image dataset are 0.9153 and 0.8314. Figure 13 shows the loss and accuracy plots for this case.

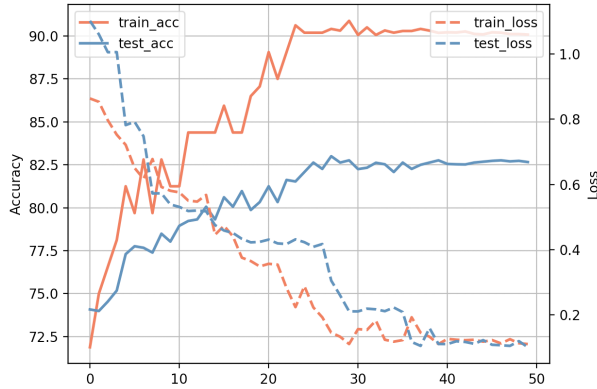


Figure 13: AlexNet performance

4.2.3 DenseNet

We built a DenseNet based on the `Keras` library. Each convolution layer is followed by a max pooling layer. Three dense blocks are used, and there is a classification layer at the end. We found that a learning rate to 0.001 and 16 filters gave the best results. We trained the model for 30 epochs. This DenseNet, when applied to our LGESS dataset, yields a training accuracy of 0.8683 and a testing accuracy of 0.8457 Figure 14 details our DenseNet performance.

4.2.4 ResNet

We also used the `Keras` library to build our ResNet. This ResNet is built with a convolution layer, max pooling layer, basic block layers, and an average pooling layer. The basic block layer includes a convolution layer, a batch normalization layer, and an activation layer. We trained our model for 20 epochs and obtained a best training accuracy of 0.9978, and testing accuracy of 0.8570. Figure 15 shows the performance of this ResNet model on our dataset.

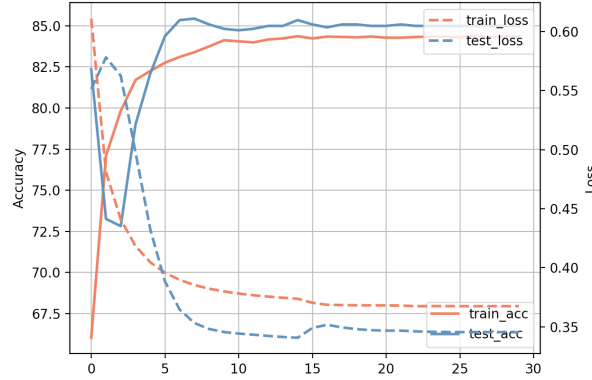


Figure 14: DenseNet performance

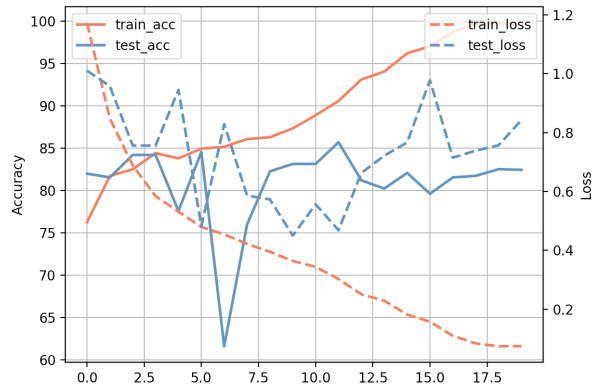


Figure 15: ResNet performance

4.2.5 ResNet with Realtime Data Augmentation

Since ResNet showed the best performance, we decided to test ResNet with realtime data augmentation. In realtime data augmentation, images in the existing dataset are copied, randomly rotated, shifted, or flipped to form an augmented dataset. ResNet with data augmentation yielded a slightly improved accuracy of 0.8788 in training and 0.8685 in testing. The accuracy and loss plots for this model are shown in Figure 16.

Figure 17 compares the training and test accuracy for each advanced technique considered in this section. We note that ResNet with real time data augmentation has the highest classification accuracy at 0.8685.

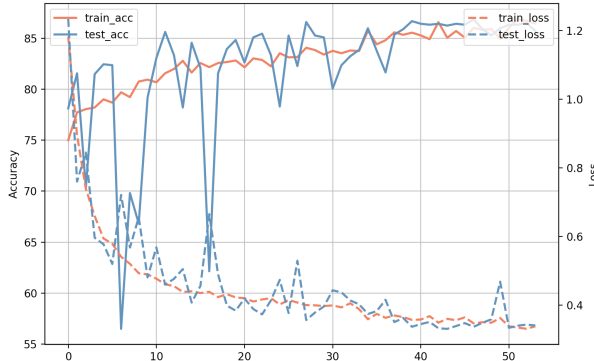


Figure 16: ResNet with data augmentation performance

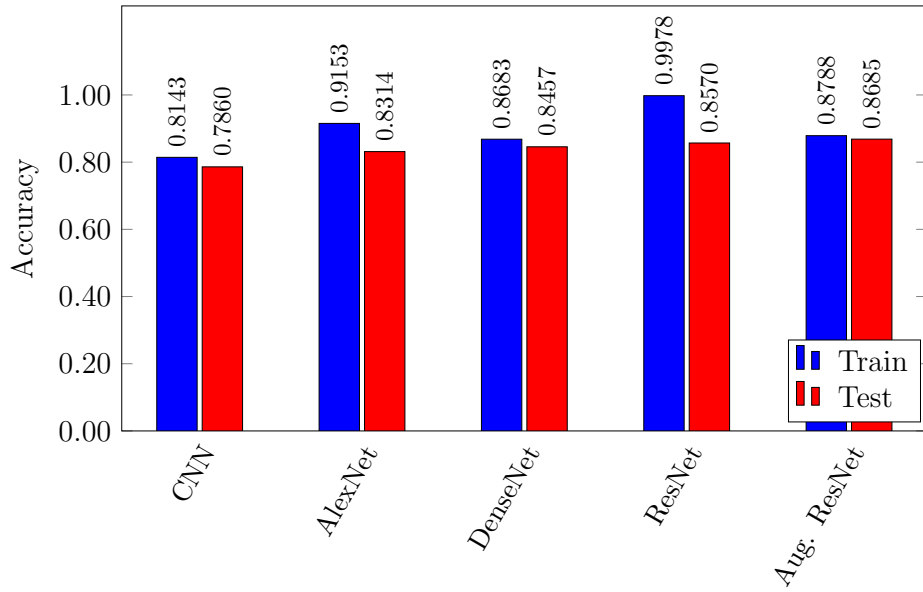


Figure 17: Accuracies for advanced techniques

4.3 Discussion

Figure 18 summarizes the test performance of all of the machine learning and deep learning algorithm we experimented with on our LGESS image database. XGBoost, SVM and PCA with SVM all yield nearly identical accuracy of 0.85, while SVM has a slight edge in terms of AUC. ResNet yielded an accuracy of 0.8570, which was improved by about 0.01 with realtime data augmentation.

Comparing our results, we see that several models perform nearly-equally well. Furthermore, accuracies in the range of 0.85 are much better than is currently achieved in practice.

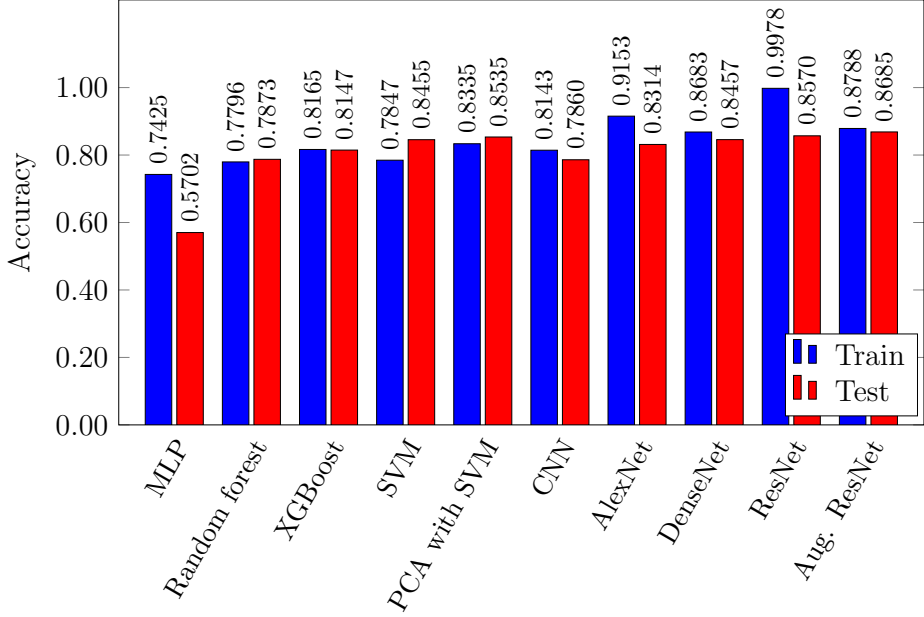


Figure 18: Test accuracy for all techniques

5 Conclusion

Cancer results in massive health care expenses and staggering death tolls [2]. Early detection of cancer can significantly reduce mortality. Therefore, fast, easy-to-use, and high precise tools for automatic cancer screening could lower healthcare costs, and ultimately save lives.

We are not aware of previous research into the efficacy of machine learning and deep learning models in screening for LGESS. Our results indicate that several models have the potential to provide accurate results in a realistic setting. Specifically, we found that XGBoost, SVM, and ResNet models could achieve accuracies of 0.85 or better.

Today, 75% of LGESS patients are incorrectly diagnosed with benign leiomyoma, leading to a delay in needed treatment and lower chances of survival. In this work, we have demonstrated that machine learning can, at a minimum, serve as a second opinion, and thereby prevent many incorrect diagnoses.

In future studies, additional characteristics can be extracted from images, which would enable learning algorithms to work with a more refined and detailed feature space. Moreover, there exists a plethora of additional machine learning and deep learning algorithms that could be considered. Such further research could benefit individuals who suffer from the rare, but potentially deadly, disease of low grade endometrial stromal sarcoma.

References

- [1] Abhimanyu S. Ahuja. The impact of artificial intelligence in medicine on the future role of the physician. *PeerJ*, page e7702, 2019.
- [2] American Cancer Society. The economic impact of cancer. <https://www.cancer.org/cancer/cancer-basics/economic-impact-of-cancer.html>, 2018.
- [3] D. Anand, G. Ramakrishnan, and A. Sethi. Fast GPU-enabled color normalization for digital pathology. In *2019 International Conference on Systems, Signals and Image Processing*, IWSSIP, pages 219–224, 2019.
- [4] Sarah Mohd Ashhar, Siti Salasiah Mokri, Ashrani Aizzuddin Abd Rahni, Aqilah Baseri Huddin, Noraishikin Zulkarnain, Nor Aniza Azmi, and Thanuja Mahaleetchumy. Comparison of deep learning convolutional neural network (CNN) architectures for CT lung cancer classification. *International Journal of Advanced Technology and Engineering Exploration*, 8:126–134, 2021.
- [5] Kristin P. Bennett and Colin Campbell. Support vector machines: Hype or hallelujah? *SIGKDD Explorations*, 2(2):1–13, 2000.
- [6] Anusha Bharat, N. Pooja, and R. Anishka Reddy. Using machine learning algorithms for breast cancer risk prediction and diagnosis. In *3rd International Conference on Circuits, Control, Communication and Computing*, I4C, pages 1–4, 2018.
- [7] Dorry Boll, Rob H. A. Verhoeven, Maaike A. van der Aa, Patrick Pauwels, Henrike E. Karim-Kos, Jan Willem W. Coebergh, and Helena C. van Doorn. Incidence and survival trends of uncommon corpus uteri malignancies in the Netherlands. *International Journal of Gynecological Cancer*, 22(4):599–606, 2012.
- [8] Leo Breiman and Adele Cutler. Random forestsTM. https://www.stat.berkeley.edu/~breiman/RandomForests/cc_home.htm.
- [9] CAMELYON16. <https://camelyon16.grand-challenge.org/Data/>, 2021.
- [10] The cancer imaging archive: National cancer institute clinical proteomic tumor analysis consortium (cptac). <https://www.cancerimagingarchive.net/>, 2018.
- [11] K. L. Chang, G. S. Crabtree, S. K. Lim-Tan, R. L. Kempson, and M. R. Hendrickson. Primary uterine endometrial stromal neoplasms. a clinicopathologic study of 117 cases. *The American Journal of Surgical Pathology*, 14(5):415–438, 1990.
- [12] Saket S. Chaturvedi, Kajol Gupta, and Prakash. S. Prasad. Skin lesion analyser: An efficient seven-way multi-class skin cancer classification using mobilenet. <https://arxiv.org/abs/1907.03220>, 2020.

- [13] Tianqi Chen and Carlos Guestrin. XGBoost: A scalable tree boosting system. <https://arxiv.org/abs/1603.02754>, 2016.
- [14] Daphne Cornelisse. An intuitive guide to convolutional neural networks. <https://medium.freecodecamp.org/an-intuitive-guide-to-convolutional-neural-networks-260c2de0a050>, 2018.
- [15] A. Gadducci, E. Sartori, F. Landoni, P. Zola, T. Maggino, and A. Urgesi. Endometrial stromal sarcoma: analysis of treatment failures and survival. *Gynecologic Oncology*, 63(2):247–253, 1996.
- [16] Ahmed Ghoneim, Ghulam Muhammad, and M. Shamim Hossain. Cervical cancer classification using convolutional neural networks and extreme learning machines. *Future Generation Computer Systems*, 102:643–649, 2020.
- [17] Maryellen L. Giger. Machine learning in medical imaging. *Journal of the American College of Radiology*, 15(3, Part B):512–520, 2018.
- [18] Kaiming He, Xiangyu Zhang, Shaoqing Ren, and Jian Sun. Deep residual learning for image recognition. In *Proceedings of the IEEE Conference on Computer Vision and Pattern Recognition*, CVPR, pages 770–778, 2016.
- [19] Healthline. What are the 12 leading causes of death in the United States? <https://www.healthline.com/health/leading-causes-of-death>, 2018.
- [20] M. R. Hendrickson, F. A. Tavassoli, R. L. Kempson, W. G. McCluggage, U. Haller, and R. A. Kubik-Huch(2003). Mesenchymal tumours and related lesions. *WHO classification of Tumours Pathology and Genetics Tumours of the Breast and Female Genital Organs*, pages 233–236, 2007.
- [21] G. Huang, Z. Liu, L. Maaten, and K. Weinberger. Densely connected convolutional networks. In *Proceedings of the IEEE Conference on Computer Vision and Pattern Recognition*, CVPR, pages 4700–4708, 2017.
- [22] Reena Jain, Swaraj Batra, Ayesha Ahmad, Arifa Anwar Elahi, Monika Gupta, and Poonam Saith. Low grade endometrial stromal sarcoma: A case report. *Iranian Journal of Medical Sciences*, 40(1):81–84, 2015.
- [23] S. Kharya, D. Dubey, and S. Soni. Predictive machine learning techniques for breast cancer detection. *International Journal of Computer Science and Information Technologies*, 4(6):1023–1028, 2013.
- [24] Alex Krizhevsky, Ilya Sutskever, and Hinton Geoffrey. ImageNet classification with deep convolutional neural networks. *Neural Information Processing Systems*, 25, 2012.
- [25] Keith Loria. Putting the AI in radiology. *Radiology Today*, 19(1):10, 2018. <https://www.radiologytoday.net/archive/rt0118p10.shtml>.
- [26] Ilias Maglogiannis, Elias Zafiropoulos, and Ioannis Anagnostopoulos. An intelligent system for automated breast cancer diagnosis and prognosis using SVM based classifiers. *Applied Intelligence*, 30:24–36, 2009.

- [27] George D. Magoulas and Andriana Prentza. *Machine Learning in Medical Applications*, pages 300–307. Springer, 2001.
- [28] MBF Bioscience. What is whole slide imaging? <https://www.mbfbioscience.com/whole-slide-imaging>, 2021.
- [29] Hengame Abbasi Mesrabadi and Karim Faez. Improving early prostate cancer diagnosis by using artificial neural networks and deep learning. In *4th Iranian Conference on Signal Processing and Intelligent Systems*, ICSPIS, pages 39–42, 2018.
- [30] OpenSlide. <https://openslide.org>, 2021.
- [31] Mandeep Rana, Pooja Chandorkar, Alishiba Dsouza, and Nikahat Kazi. Breast cancer diagnosis and recurrence prediction using machine learning techniques. *International Journal of Research in Engineering and Technology*, 04(04):372–376, 2015.
- [32] Pietro Renzulli, Rosemarie Weimann, Jean-Pierre Barras, Thierry-Pierre Carrel, and Daniel Candinas. Low-grade endometrial stromal sarcoma with inferior vena cava tumor thrombus and intracardiac extension: radical resection may improve recurrence free survival. *Surgical Oncology*, 18:57–64, 2009.
- [33] Mihir Sewak, Priyanka Vaidya, Chien-Chung Chan, and Zhong-Hui Duan. SVM approach to breast cancer classification. In *Second International Multi-Symposiums on Computer and Computational Sciences*, IMSCCS, pages 32–37, 2007.
- [34] Jonathon Shlens. A tutorial on principal component analysis. <http://www.cs.cmu.edu/~elaw/papers/pca.pdf>.
- [35] Abhishek Vahadane, Tingying Peng, Amit Sethi, Shadi Albarqouni, Lichao Wang, Maximilian Baust, Katja Steiger, Anna Melissa Schlitter, Irene Esposito, and Nassir Navab. Structure-preserving color normalization and sparse stain separation for histological images. *IEEE Transactions on Medical Imaging*, 35(8):1962–1971, 2016.
- [36] R. Vijayarajeswari, P. Parthasarathy, S. Vivekanandan, and A. A. Basha. Classification of mammogram for early detection of breast cancer using SVM classifier and Hough transform. *Measurement*, 146:800–805, 2019.
- [37] Charles Wallis. History of the perceptron. <https://web.csulb.edu/~cwallis/artificialn/History.htm>, 2017.